Journal of Astronomical Telescopes, Instruments, and Systems

AstronomicalTelescopes.SPIEDigitalLibrary.org

Thermal control for light-weighted primary mirrors of large ground-based solar telescopes

Naiting Gu
Cheng Li
Yuntao Cheng
Changhui Rao

SPIE.

Naiting Gu, Cheng Li, Yuntao Cheng, Changhui Rao, "Thermal control for light-weighted primary mirrors of large ground-based solar telescopes," *J. Astron. Telesc. Instrum. Syst.* **5**(1), 014005 (2019), doi: 10.1117/1.JATIS.5.1.014005.

Thermal control for light-weighted primary mirrors of large ground-based solar telescopes

Naiting Gu,[a,b,*] Cheng Li,[a,b] Yuntao Cheng,[a,b] and Changhui Rao[a,b,*]
[a]Chinese Academy of Sciences, Institute of Optics and Electronics, Chengdu, China
[b]Chinese Academy of Sciences, The Key Laboratory on Adaptive Optics, Chengdu, China

Abstract. A light-weighted primary mirror is the most important optical element for a large ground-based solar telescope. It receives solar radiation of more than 1000 W/m^2, of which about 10% is converted into heat energy, bringing in mirror seeing effect and surface shape distortion. Thus, a thermal control system (TCS) is necessary and important. Many studies have discussed the factors that influence the temperature difference between mirror surface and ambient air, but few refer to TCS modeling and optimization for the sake of parameter estimation. A thermal control model for the parameter estimation is proposed. The analytical process and the numerical analysis results of the model on the Chinese large ground-based solar telescope are given. A 60-cm prototype of open solar telescope (POST) is developed, on which practical experiment is taken place. According to the parameters estimated results, we select devices for the TCS of the POST. The experiment results show that the maximum temperature difference was restricted within ±0.5°C, despite the temperature variation of the ambient air, whereas without TCS, the maximum temperature difference rises up to 6.5°C. That validates the feasibility and effectiveness of the proposed model, and it can be referred for other large ground-based solar telescopes. [DOI: 10.1117/1.JATIS.5.1.014005]

Keywords: mirror seeing; thermal control system; primary mirror; ground-based solar telescope.

Paper 18045 received Aug. 1, 2018; accepted for publication Jan. 23, 2019; published online Feb. 12, 2019.

1 Introduction

With the progress in solar physics, higher spatial resolution is required in observing solar active regions to understand smaller-scale physical processes in the solar atmosphere. By theoretical calculation, the scale of magnetic fine structures in the solar atmosphere, for example, the flux tube, is smaller than 70 km.[1] To observe it, the angle resolution of a solar telescope should be finer than 0.1 arc sec.[1] In other words, the aperture of a solar telescope should be larger than 1 m to observe magnetic fine structures in the solar atmosphere. Moreover, with a telescope of a small aperture, the photo hungry polarization measurements could hardly be carried out, which are crucial to estimate the distribution and strength of magnetic fields in the solar active regions.[2,3]

Many large solar telescopes have been built, such as the 1.6-m McMath–Pierce solar telescope,[4] the 1.5-m GREGOR solar telescope,[5] and the 1.6-m new solar telescope.[6] And there are more planned, such as the 4-m Daniel K. Inouye solar telescope,[7] the 4-m European solar telescope,[8] the 2-m National large solar telescope,[9] and the 1.8-m Chinese large solar telescope.[10]

The design and construction of large solar telescopes are considerably different from small (1 m and smaller) ones. Large solar telescopes utilize an open structure, which is cost saving and avoids the issue of sealing and stress birefringence. Compared to a vacuum tube, the imaging quality of solar telescope with an open structure design will be threatened by mirror seeing and internal seeing effects, which are generated from the temperature difference between the optical or mechanical elements and the ambient air. The primary mirror of an open solar telescope is heated by intensive solar radiation. The temperature difference between the mirror surface and the ambient air brings in the mirror seeing effect and a mirror deformation, thus introducing a dynamic wavefront aberration, which degrades the imaging quality of the solar telescope. Thus, a thermal control system (TCS) for the primary mirror is crucial for large solar telescopes, which can minimize the temperature difference between the mirror surface and the ambient air. Many studies have intensively discussed the factors that influence the temperature difference between the mirror surface and the ambient air,[11–13] and several practical TCSs are discussed.[14–19] But, few refer to a TCS modeling and optimization for the sake of parameter estimation and device selection, especially for ground-based solar telescopes.

This paper proposes a thermal control model for the parameter estimation of the TCS. The analytical derivation process of the model and the numerical analysis results of the model for the Chinese large ground-based solar telescope (CLST) are also given. To demonstrate the feasibility and effectiveness of the thermal control model, a 60-cm prototype of the open solar telescope (POST) had been developed, on which the practical experiments had been performed. According to the parameters estimated by the proposed thermal control model, we select devices for the TCS of the POST. The practical experiment results show that the TCS of the POST restricts the maximum temperature difference between the mirror surface and the ambient air within ±0.5°C, despite the temperature variation of the ambient air. And without the TCS, the maximum temperature difference rises up to 6.5°C. In conclusion, the proposed thermal control model is feasible and effective and can be referred to in the engineering of the TCS of large ground-based solar telescopes, such as the CLST.

*Address all correspondence to Naiting Gu, gnt7328@163.com; Changhui Rao, chrao@ioe.ac.cn

This paper is organized as follows: Sec. 2 briefly introduces the CLST and its TCS. Section 3 presents our thermal control model through analytical derivation and Sec. 4 validates the model on the CLST through numerical analysis. Section 5 describes the POST and gives the practical experiment results of the proposed-model optimized TCS, including the optimized air pressure. We make a conclusion and discuss the future work in Sec. 6.

2 CLST and its Thermal Control System for the Primary Mirror

To better understand and forecast the solar activities and its impacts on human technologies and life on earth, an 1.8-m solar telescope CLST was proposed in 2011.[20,21] According to the original schedule, the CLST should be built and put into operation by 2017. However, the project was postponed due to financial problems. According to the latest schedule, the CLST is under construction and will be completed by the end of 2019. The optical system and the support structure (including mount and tube truss) of the CLST are shown in Fig. 1.

The CLST was designed as an open telescope by using the Gregorian optical configuration, with an alt-azimuth mount, a retractable dome, and a large mechanical derotator. The aperture size of the CLST is 1800 mm. And the field-of-view is up to 6 arc min. The CLST utilizes a relay optics system similar to the GREGOR solar telescope, which minimizes instrumentation polarization. A solar adaptive optics system is developed to enable diffraction-limited observations at visible and infrared wavelengths. A multiwavelength tomographic imaging system with seven wavelengths ranging from visible to near-infrared will operate as the first light instruments of the CLST.

The primary mirror is the key optics element of the CLST, as shown in Fig. 2. It is made of ULE material and consists of a face sheet, a honeycomb sandwich layer, and a back sheet. The thickness of the face sheet is 20 mm, well balanced between thermal transmission and stiffness. The radius of curvature of the face sheet is 7120 mm, and the focal ratio is 1.7.

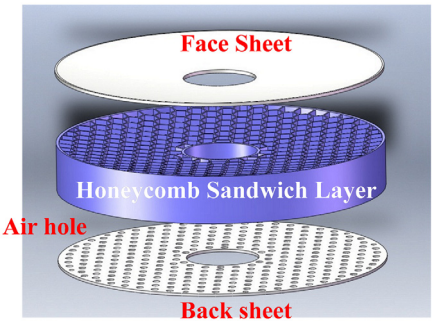

Fig. 2 The component diagram of the light-weighted primary mirror of CLST.

The honeycomb sandwich layer consists of 297 hexagonal cavities, and each is paired to a hole in the back sheet.

The face sheet of the primary mirror utilizes a protecting aluminum coating, through which about 10% of the incident solar radiation is transferred into heat, further adding to the mirror seeing effect. To reduce the mirror seeing effect, the CLST utilizes a TCS, as shown in Fig. 3.

The TCS consists of three identical and independent units, each works for a 120 deg sector of the primary mirror. There are 297 inflow nozzles (IN), over 100 return flow nozzles (RFN), and 3 integrated ventilators totally. The integrated ventilator consists of a ventilator, a heat exchanger (HE), and a heater. The main components and the assembly of one unit of the TCS are illustrated in Fig. 3.

The INs are inserted into the cavities of the honeycomb sandwich layer through the holes in the back sheet. The ventilators are used to inject air through INs into the cavities to cool the bottom of the face sheet. The air is guided back through the RFNs and cooled in the HEs integrated in the ventilators. This is a closed air circulation in the primary mirror. The HEs are liquid cooling using glycol water solution as coolant. The heated liquid from HEs is cooled by a refrigerating machine.

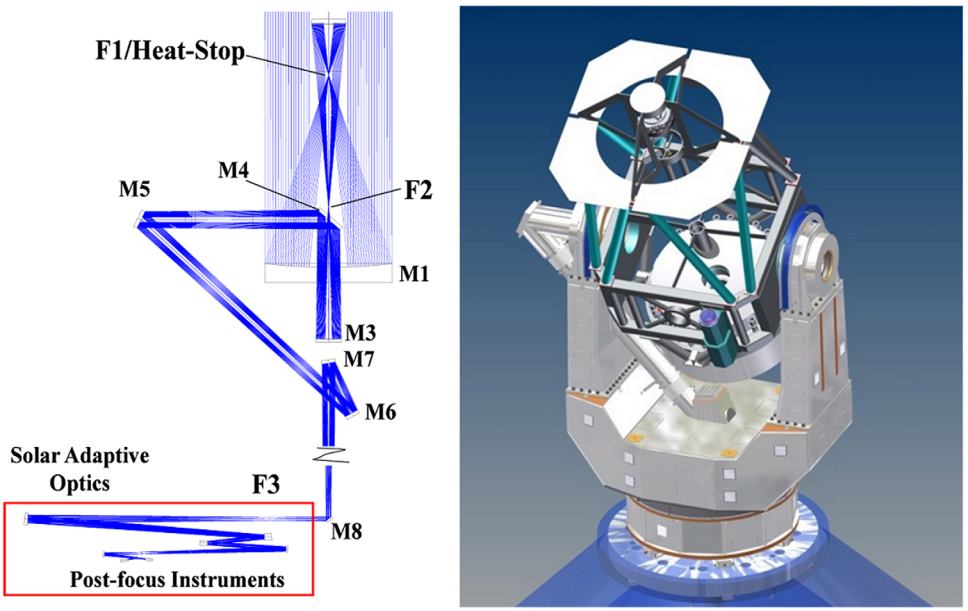

Fig. 1 Optical configuration and support structure (including mount and tube truss) of CLST.

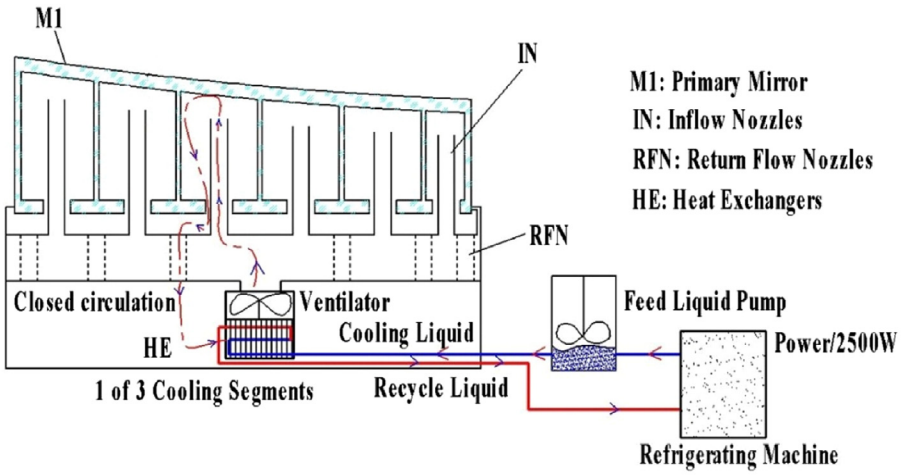

Fig. 3 The component diagram of the TCS for the primary mirror of CLST.

There are two factors that affect the temperature difference of the mirror surface and the ambient air: (a) the flow rate of the ventilators and (b) the temperature of the injected air. In practical systems, fix frequency ventilators are preferred to avoid additional jitter introduced by frequency changing. Therefore, the temperature difference can be adjusted by changing the flow rate of coolant, the temperature of coolant, and the power of the heater.

3 Thermal Control Model for the Primary Mirror

As shown in Figs. 2 and 3, there are 297 cavities with an inserted IN. Each cavity can be considered as a cell of the TCS. Most cells are identical except the ones along the edge of the primary mirror. As shown in Fig. 4(a), the diameter of the hexagonal cavity is D. An IN with internal diameter of d is located at the center of the cavity, whose tip is H below the bottom of the face sheet [as shown in Fig. 4(b)]. For simplicity, three assumptions are made as follows: (a) All the units are of the same D, d, l, and H; (b) the radius of curvature of the primary mirror is large enough, and the portion to each cell can be approximated to a plane; (c) solar radiation is either reflected or absorbed by the face sheet without regard for black-body radiation.

Assuming that there is no wind, as the worst case, only natural convection from the mirror surface to the ambient air exists. As shown in Fig. 4(b), the heat transfer process at the face sheet includes: (a) thermal absorption (i.e., Φ_a), which is the residual power of the solar radiation Φ_s after reflecting from the mirror surface; (b) natural convection between the surface and the ambient air, i.e., Φ_n; (c) thermal conduction from the surface to the bottom, i.e., Φ_c; and (d) forced air convection heat transfer between the IN-injected cool air and the bottom of the face sheet. For simplification, we will analyze the heat transfer

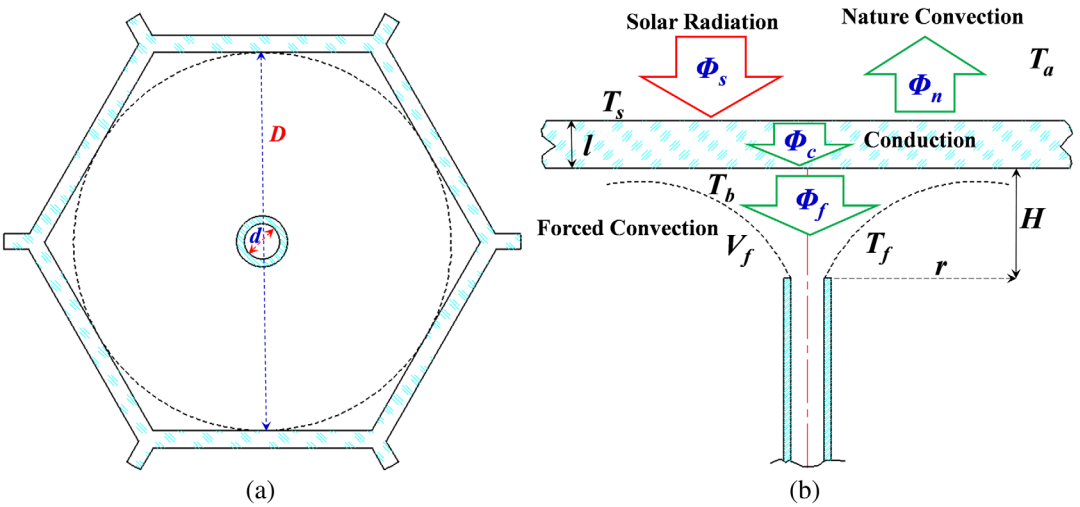

Fig. 4 The cross-section diagram of a hexagonal cavity in the honeycomb sandwich layer and illustration of the air forced cooling process. (a) The cross-section diagram of a hexagonal cavity (D-diameter of the incircle; d-internal diameter of IN). (b) Illustration of the air forced cooling process for each cavity (Φ_s, power of solar radiation; Φ_n, air nature convection from the surface of the face sheet; Φ_c, heat conduction; Φ_f, air forced convection from the bottom of the face sheet; H, distance from the tip of IN to the bottom of the face sheet; l, thickness of the face sheet; T_s and T_b, the temperature of the surface and the bottom of the face sheet; T_a and T_f, the temperature of the ambient air and the air injected through the IN; V_f, air inflow velocity).

process based on one classical cell but not on the entire mirror. The power density of solar radiation is 1000 to 1300 W/m^2 according to the site of a ground-based solar telescope, and the thermal absorption Φ_a can be presented as follows:

$$\Phi_a = \eta\rho A = \eta\Phi_s, \tag{1}$$

where η is thermal absorption coefficient (5% to 10% according to the coating of the mirror surface), ρ is the power density of solar radiation, and A is the cross-sectional size of the hexagonal cavity.

According to the first law of thermodynamics (i.e., the law of conservation of energy), the heat transfer process can be presented as follows:

$$\Phi_a - \Phi_n = \Phi_c = \Phi_f, \tag{2}$$

where

$$\Phi_n = h_n A(T_s - T_a), \tag{3}$$

$$\Phi_c = \frac{\lambda_c}{l} A(T_s - T_b), \tag{4}$$

$$\Phi_f = h_f A(T_b - T_f), \tag{5}$$

where h_n and h_f are the heat transfer coefficients of the air natural convection and the forced air convection, respectively; λ_c is the thermal conductivity of the face sheet; l is the thickness of the face sheet; T_s and T_b are the temperatures of the surface and the bottom of the face sheet; T_a and T_f are air temperatures of the ambient air and the air injected through IN.

By synthesizing Eqs. (1)–(5), a new equation can be deducted as follows:

$$T_s - T_a = \frac{\eta\rho\left(\frac{l}{\lambda_c} + \frac{1}{h_f}\right) + (T_f - T_a)}{h_n\left(\frac{l}{\lambda_c} + \frac{1}{h_f} + \frac{1}{h_n}\right)}. \tag{6}$$

For a TCS, the main task is to minimize the mirror seeing effect, and the controlling goal is also to minimize the temperature difference between the mirror surface and the ambient air, i.e., $T_s - T_a$ should be close to 0. Thus, the required parameters of the TCS can be estimated when the idealization goal is satisfied. A new thermal control equation can be presented as follows:

$$T_f = T_a - \eta\rho\left(\frac{l}{\lambda_c} + \frac{1}{h_f}\right). \tag{7}$$

For a certain ground-based solar telescope, l and η are constants; ρ and T_a are measurable time-varying variables. Deriving form Eq. (7), the ideal temperature of the air injected by IN T_f is a function of ρ, T_a, and h_f. h_f is a certain average heat-transfer coefficient, which can be calculated by the model of air forced convection of single circle nozzle with internal diameter of r:[22]

$$\frac{h_f d}{\lambda_a} = (Nu_d)_m = 2Re_d^{0.5}Pr^{0.42}(1 + 0.005Re_d^{0.55})^{0.5} \times \frac{1 - 1.1d/r}{1 + 0.1(H/d - 6)d/r}\frac{d}{r}, \tag{8}$$

where

$$Re_d = \frac{V_f d}{v}, \tag{9}$$

where $(Nu_d)_m$ is the average Nusselt number; Re_d is the Reynolds number with characteristic length d; Pr is the Prandtl number of air; λ_a is the thermal conductivity of the injected air; V_f is the flow velocity at the tip of an IN; and v is the dynamic viscosity.

Substituting Eqs. (8) and (9) in Eq. (7), we can get Eq. (10) as follows:

$$T_f = T_a - \eta\rho\left(\frac{l}{\lambda_c} + \frac{d}{F\{V_f\}\lambda_a}\right), \tag{10}$$

where

$$F\{V_f\} = 2Pr^{0.42}\frac{1 - 1.1d/D}{1 + 0.1(H/d - 6)d/D} \times \frac{d}{D}\sqrt{\frac{V_f d}{v} + 0.005\left(\frac{V_f d}{v}\right)^{1.05}}. \tag{11}$$

According to Eqs. (7) and (10), T_s changes with V_f and T_f as T_a varies by time. In other words, the temperature of the mirror surface can be controlled by adjusting the flow rate of the ventilator and the temperature of the injected air. In practical systems, fix frequency ventilators are preferred to avoid additional jitter introduced by frequency changing. Therefore, the temperature of the mirror surface can be controlled by adjusting only the temperature of the injected air T_f. The selection of the ventilator frequency and the temperature range of the injected air should be well balanced too. The relationship of V_f and the air flow rate of the ventilator Ω can be expressed as follows:

$$V_f = \frac{1}{N}\frac{1}{\pi(d/2)^2}\Omega(P), \tag{12}$$

where N is the number of INs and $\Omega(P)$ is the flow rate of the selected ventilator with the air pressure P.

For a certain ground-based solar telescope, some variables in Eqs. (10) and (11) (such as the thermal absorption coefficient η, thickness of the face sheet l, the internal diameter d of IN, the incircle diameter D of hexagonal cavity, the distance H from the IN tip to the bottom of the face sheet, the thermal conductivity λ_c of the face sheet, the thermal conductivity λ_a of the injected air, and the dynamic viscosity-v) can be approximated to constants within a narrow temperature range. The Prandtl number Pr is not strongly dependent on pressure and temperature, and it can be considered as a constant over a fairly wide range of pressure and temperature.[23] The power density of the solar radiation ρ and the temperature of the ambient air T_a are measurable variables relevant to the site and time. The power density of the solar radiation ρ can be calculated by[24]

$$\rho = \rho_0(\sin\delta\sin\phi + \cos\delta\cos\phi\cos\theta_H), \tag{13}$$

where[25]

$$\theta_H = \frac{\pi}{12}(t - 6) - \frac{\pi}{2}, \quad \delta = 23.45\sin\left(360\frac{284 + n}{365}\right), \tag{14}$$

where ρ_0 is the power density of the solar radiation when the observatory site is located at the equator and when the sun is at zenith, ϕ is the latitude of the selected site, δ is the declination angle of the sun, θ_H is the solar hour angle with respect to noon, n is the day of the year, and t is the local time.

For a certain site, the temperature at daytime can be calculated by[24]

$$T_a(t) = s \times \begin{cases} T_0 + T_b \cos\left[\frac{\pi}{\omega}(t-\tau_m)\right], & \text{for } t < t_s \\ T_0 + \delta T + \left[T_b \cos\frac{\pi}{\omega}(t-\tau_m) - \delta T\right] e^{-\frac{t-t_s}{k}}, & \text{for } t \geq t_s \end{cases}, \quad (15)$$

where T_0 (°C) is the residual temperature at sunrise, T_b (°C) is the temperature amplitude, ω is the half oscillation period of cosine term, τ_m is the time when the maximum temperature is reached, t_s is the time when temperature attenuation begins, s is scaling factor, $\delta T = T_0 - T(t \to \infty)$, and k is the attenuation constant.

With the above mentioned equations, we can make a well-balanced selection of the flow velocity V_f of the ventilator and the temperature range of the injected air T_f, according to Eq. (10).

4 Numeric Analysis of the Thermal Control Model on the CLST

The site of the CLST is Wuming Mountain in Dao city, Sichuan province, China. On the site, the peak solar flux is over 1200 W/m^2 and the ambient air temperature at daytime is ranging from 5°C to 15°C in summer. According to the theoretical analysis in Sec. 3, we make a numerical analysis on the CLST in order to optimize the TCS of its primary mirror.

Table 1 lists the values of the required thermal parameters for Eqs. (10) and (11). Table 2 gives the values of required dimensional parameters for Eqs. (11) and (12).

The numeric analysis is performed for a clear day. The solar radiation is continuous from sunrise (6:00 am) to sunset (18:00 pm) and the solar flux at the site reaches 1200 W/m^2 maximum at noon (12:00). The thermal time lag between the maxima of the solar flux and the ambient air temperature is about 2 h, which means the ambient air temperature continues to rise until 14:00 pm. More parameters are listed in Table 3.

The estimated solar flux and the temperature of the ambient air during a clear day are shown in Fig. 5. As we can see, due to thermal time lag in a terrestrial environment, the temperature of the ambient air continues to rise after the solar noon.

Putting the values listed in Tables 2–4 into Eqs. (10) and (11), the relationship between the optimal temperature of the injected air T_f and the flow velocity V_f can be calculated. In this paper, we assume that the primary mirror of the CLST is at the same temperature of the ambient air at sunrise (6:00 am) and sunset (18:00 pm) and calculate the optimal temperature of the injected

Table 1 Values of thermal parameters for Eqs. (10) and (11).[23]

Parameter	Meaning	Values	Units
λ_c	Thermal conductivity of face sheet (ULE)	1.31	W/(mK)
λ_a	Thermal conductivity of the injected air	2.51×10^{-2}	W/(mK)
v	Dynamic viscosity	1.416×10^{-5}	m^2/s
Pr	Prandtl number	0.705	—
h_n	Heat transfer coefficient of air nature convection	5	W/(m^2°C)

Table 2 Values of dimensional parameters for Eqs. (11) and (12).

Parameter	Meaning	Values	Units
η	Thermal absorption coefficient of the primary mirror (protected Al coating)	10%	—
L	Thickness of the face sheet of the primary mirror	20	mm
d	Internal diameter of IN	20	mm
D	Incircle diameter of a hexagonal cavity	90.1	mm
H	Distance from the IN tip to the bottom of the face sheet	30	mm
N	The number of INs	297	—

Table 3 Values of parameters for solar flux and the ambient temperature calculation.

Parameter	Meaning	Values	Units
ρ_0	The power density of solar radiation when the sun is at zenith/	1376	W/m^2
ϕ	Latitude of the selected site	N29.15	°
n	The day of the year	135	—
δ	Declination angle of the sun [calculated by Eq. (14)]	18.8	°
θ_H	Solar hour angle with respect to noon	$-\pi/2$ to $+\pi/2$	—
t	Local time	06:00 to 18:00	h
T_0	Residual temperature at sunrise	8.33	°C
T_b	Temperature amplitude	6.67	°C
ω	Half oscillation period of cosine term	12	H
τ_m	Time when the maximum temperature is reached	14:00	h
t_s	Time when temperature attenuation begins	18:00	h
s	Scaling factor	1	—
δT	$T0$-$T(t \to \infty)$	–3.25	°C
k	Attenuation constant	3.5	h

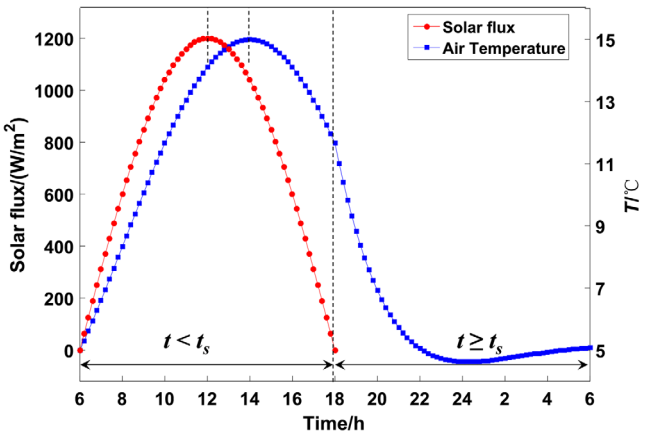

Fig. 5 The estimated solar flux and the temperature of the ambient air.

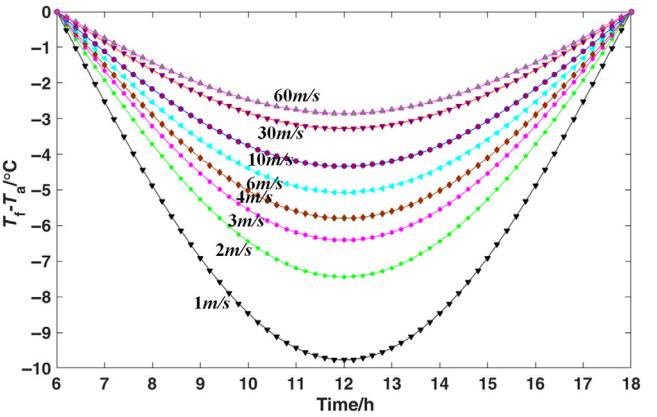

Fig. 7 Optimal temperature difference of the injected air and the ambient air at different flow velocities during daytime.

Table 4 Dimensional parameters of the TCS of the POST.

Parameter	*H*	*D*	*d*	*H*	*L*	*N*	ϕ
Value	10%	90.1 mm	15 mm	20 mm	20 mm	36	N26.71°

air during the daytime at 14 fixed flow velocities, which are 1, 2, 3, 4, 6, 8, 10, 15, 20, 25, 30, 40, 50, and 60 m/s, respectively. Although some of them seem to be unpractical, they will help us to make a good conclusion in theory.

The calculation result is shown in Fig. 6. As shown, the lower the inflow velocity is, the lower the optimal temperature of the injected air is, thus requiring higher power of the refrigerating machine. That is, the power of the refrigerating machine can be brought down by selecting the ventilator with higher inflow velocity. However, as selected inflow velocity gets higher, its benefit in power saving for the refrigerating machine keeps declining, as shown in Fig. 7. So, the selection of the inflow velocity should be well balanced.

Figure 8 shows the maximum temperature differences required of the injected air and the ambient air at selected inflow velocities, where larger temperature difference means higher refrigerating machine power. It resembles a logarithmic curve, which implies the well-balanced solution is within the inflow velocity from 6 to 8 m/s, where the maximum temperature difference of the injected air and the ambient air is from −5.07°C to −4.64°C. Put the values in Table 2 into Eq. (12), we can learn

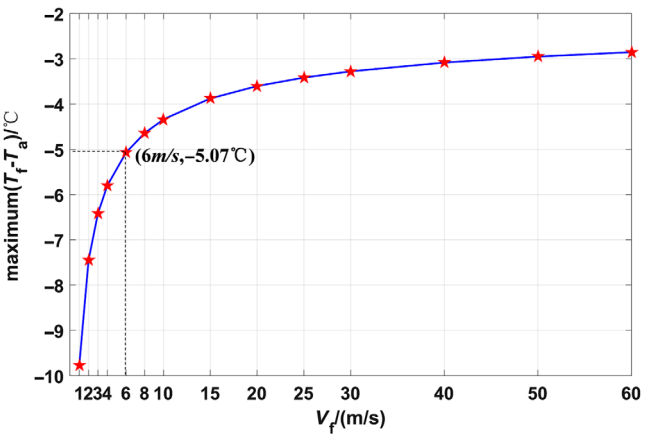

Fig. 8 Maximum temperature differences required at selected inflow velocities.

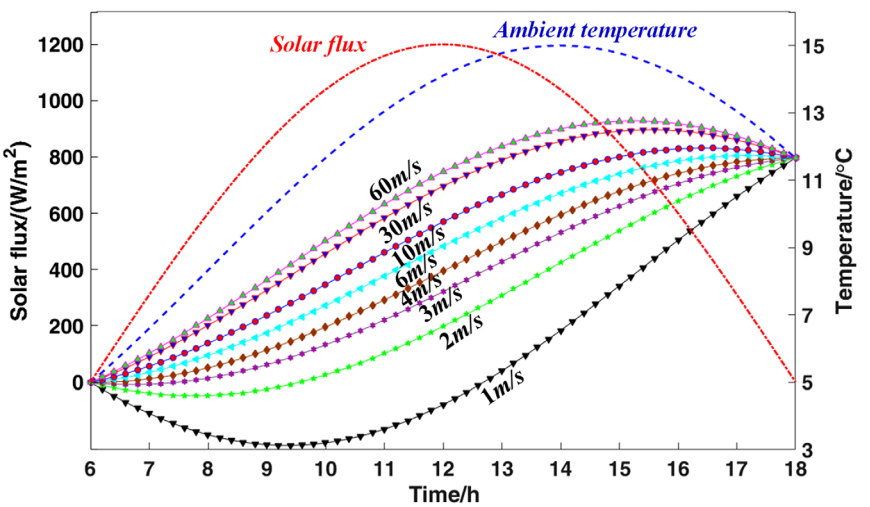

Fig. 6 Optimal temperature of the injected air at different flow velocities during daytime.

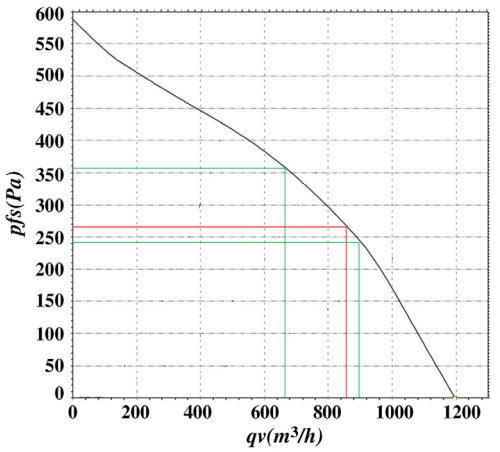

Fig. 9 The flow rate and air pressure required for candidate ventilators (red lines indicate the candidate ventilator for the POST with 265 Pa air pressure and green lines indicate the candidate ventilators for CLST with inflow velocity of 6 and 8 m/s at the IN tips).

that the flow rate produced by three ventilators totally should be from 2015.4 to 2687.2 m^3/h, which makes the flow rate of each ventilator from 671.8 to 895.7 m^3/h.

In the practical experiment (see Sec. 5), we select a ventilator of shelf-product for the prototype based on the thermal control model. Its nominal maximum flow rate is 1200 m^3/h at 0 Pa air pressure and about 855 m^3/h at 265 Pa air pressure as the red line shown in Fig. 9. As we can see, it is also a well-balanced solution for the CLST. With this ventilator, we propose a semiconductor refrigerating machine for the TCS of the CLST, which provides a 10℃ maximum temperature difference.

5 Experimental Results on the POST

To demonstrate the feasibility and effectiveness of the thermal control model, a 60-cm POST is developed and tested in Gaomeigu Observatory (E100°01'51", N26°42'32") in Lijiang City, Yunnan Province, China. Figure 10 shows the optical configuration and the components of the POST. The hexagonal cavity of the POST is the same as the CLSTs. The internal diameter of the IN is 15 mm, and the distance from the IN tip to the bottom of the face sheet is 20 mm. More parameters are listed in

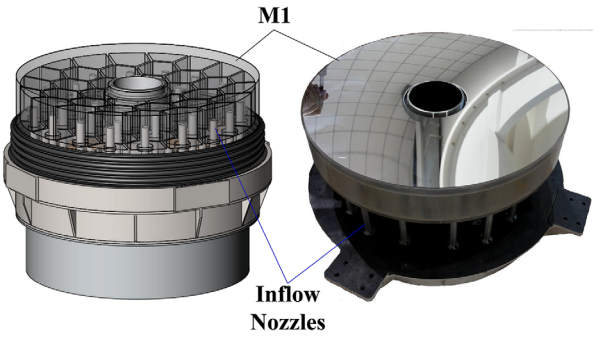

Fig. 11 Design diagram and a picture of the TCS of the POST.

Table 4. Figure 11 shows the design and a picture of the TCS of the POST.

According to the numerical analysis in Sec. 4, the maximum temperature difference required for the injected air and the ambient air of the POST can be calculated, as shown in Fig. 12.

As shown in Fig. 12, 6 m/s of inflow velocity is a well-balanced value with a maximum temperature difference of −5.5℃. According to Eq. (12), the required air flow rate is about 137 m^3/h. The air pressure is estimated to be 250 Pa roughly.

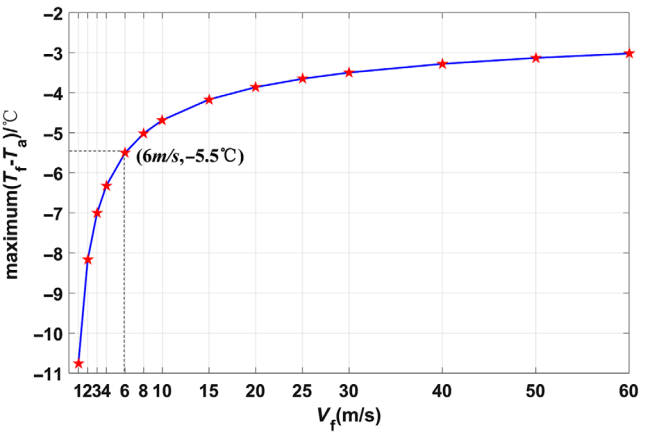

Fig. 12 The maximum temperature difference required at fixed inflow velocities of the injected air.

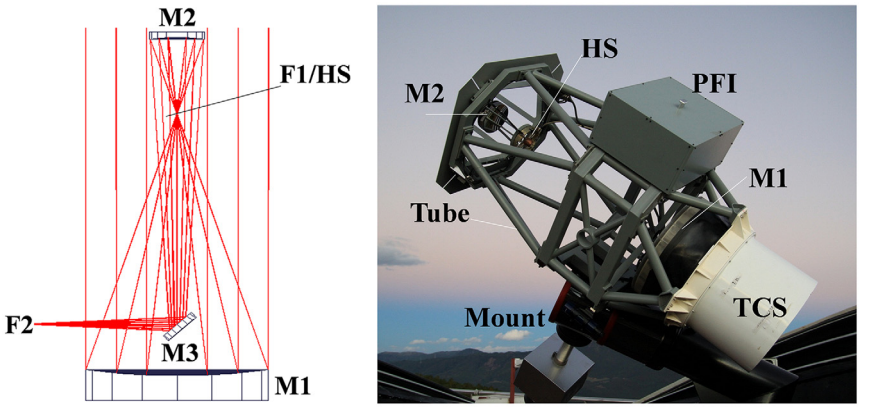

Fig. 10 (a) Optical configuration and (b) the components of the POST. M1, primary mirror; M2, secondary mirror; M3, fold mirror; F1, primary focus; F2, instrumental focus; HS, heat-stop; PFI, postfocus instruments.

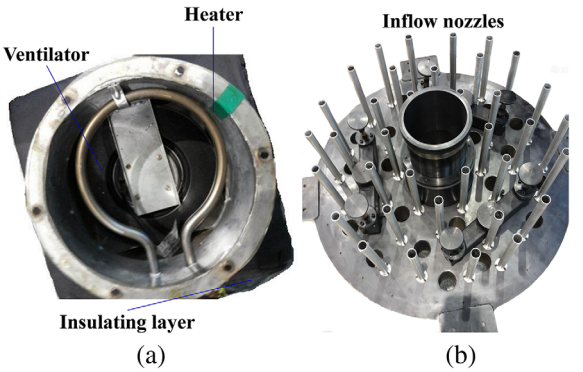

Fig. 13 (a) The integrated ventilator and (b) the refrigerating machine for the POST.

With these estimated parameters, a ventilator produced by the company *ebmpapst* in Germany (model No. R2E190A02605) is selected, which can produce a maximum air flow of 190 m^3/h. We integrate the ventilator with a heater and equip it to the TCS of the POST, as shown in Fig. 13. We tested the air velocity at each IN of the POST, which ranges from 4.53 to 4.95 m/s with an average of 4.73 m/s. The air flow rate at the air velocity can be calculated, which is about 108.33 m^3/h, and the air pressure is 265 Pa according to the user manual of the ventilator. As the TCS of the POST is similar to the one of the CLST, the air pressure of 265 Pa can be taken as a direction in the ventilator selection for the CLST.

The experiment results deviate a little from the calculated result in Fig. 12 (6 m/s, −5.5°C). However, the selected ventilator is still applicable, provided that the refrigerating machine is able to produce a larger maximum temperature difference (5.91°C). Considering a heat loss in the thermal control process, a semiconductor refrigerating machine produced by Tianjin Jingie Industry and Trade Co. Ltd. in China is selected for the TCS of the POST, which can produce a maximum temperature difference of 8°C.

We test the performance of the TCS of the POST with the selected devices. Three temperature sensors (FLUK, Pt100) of high accuracy (finer than ±0.05°C) are deployed to monitor the temperature at different points on the mirror surface. The average of the readings is taken as the temperature of the mirror surface. Figure 14 shows the temperature tracking results with and without the working of TCS. We can see that the TCS well controls the temperature difference between the mirror surface

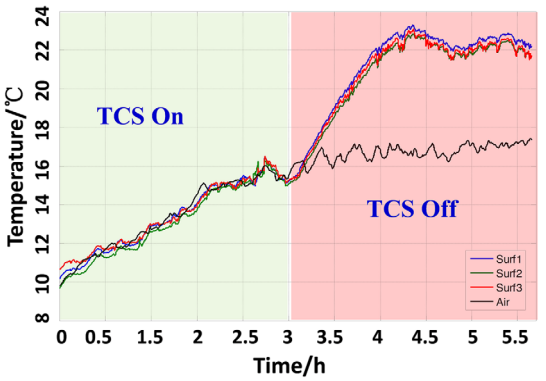

Fig. 14 Temperature of the surface of the primary mirror with and without the TCS (surf1/2/3, temperatures at three different points of the mirror surface; air, temperature of the ambient air).

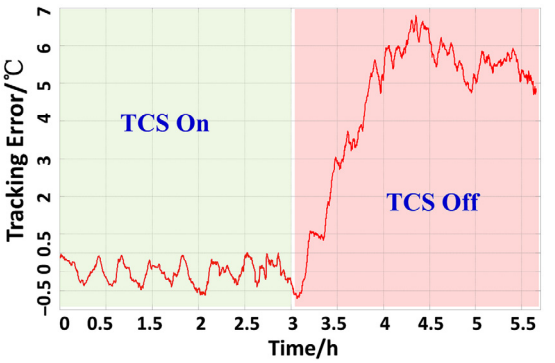

Fig. 15 Temperature tracking error of the primary mirror surface.

and the ambient air. The temperature tracking error during the experiment is shown in Fig. 15.

According to the experimental result with the TCS, the temperature difference between the mirror surface and the ambient air was controlled within ±0.5°C almost all the time and the mirror seeing effect is well reduced. On the contrary without the TCS, the temperature of the mirror surface rises up rapidly and is higher than the ambient air by 6.5°C maximum.

6 Conclusion

Thermal control is one of the most important techniques for ground-based large solar telescopes. How to optimize the TCS to well control the temperature of the mirror surface is not focused enough. In this paper, we introduce an active thermal control model through analytical derivation and application to the CLST by numerical analysis. A 60-cm POST is built to validate the thermal control model. According to the experiment results, the temperature difference between the mirror surface and the ambient air is controlled within ±0.5°C almost all the time. Without the TCS, the maximum temperature difference rises up to 6.5°C. From the experiment, we can conclude that the proposed thermal control model is feasible and effective for the engineering and device selection of the TCS and can be referred to by the CLST and other large ground-based solar telescopes.

The proposed model needs further improvements in the future such as considering heat conversion efficiency from the refrigerating machine to the injected air, temperature homogeneity control of the mirror surface, etc. Moreover, Eq. (8) is not validated experimentally on the CLST, where the value of H/d is 1.5.[23] As the consequence, Eq. (10) is a rough calculation of the parameters as well as the resulting device selection. This will bring inaccuracy to the TCS of the CLST. This is an important endeavor of our future work.

Acknowledgments

The 1.8-m CLST solar telescope is funded by the Hi-tech Project of China. The study on the TCS of the primary mirror is supported by the National Natural Science Foundation of China under the Grant Nos. 11643008 and 11727805. We would like to thank Mr. Ming Zhang, Professor Yongjian Wan, Dr. Changjun Wang, Mr. Cheng Su, Dr. Xiaoan Chen, Professor Xuedong Cao, Mr. Jinlong Huang, Dr. Yangyi Liu, Dr. Zhiyong Wang, Dr. Benxi Yao, etc. at the Institute of Optics and Electronics (IOE) of Chinese Academy of Science (CAS) for their co-operation and important help. Professor Wenhan Jiang from IOE, CAS, is also acknowledged for his good suggestions and special supports. We also appreciate to

thank the reviewers for their careful revisions and constructive comments, which helped to improve the quality of this paper.

References

1. O. Von Der Lühe et al., "GREGOR: a 1.5 m telescope for solar research," *Aston. Nachr.* **322**, 353–360 (2001).
2. R. K. Banyal and B. Ravindra, "Thermal characteristics of a classical solar telescope primary mirror," *New Astron.* **16**, 328–336 (2011).
3. D. M. Harrington, J. R. Kuhn, and A. L. Ariste, "Daytime sky polarization calibration limitations," *J. Astron. Telesc. Instrum. Syst.* **3**(1), 018001 (2017).
4. F. T. Watson et al., "Cross-calibrating sunspot magnetic field strength measurement from the McMath-Pierce solar telescope and the Dunn solar telescope," *Solar Phys.* **290**(11), 3267–3277 (2015).
5. W. Schmidt et al., "The 1.5 meter solar telescope GREGOR," *Astron. Nachr.* **333**(9), 796–809 (2012).
6. P. R. Goode et al., "1.6 M Solar telecope in big bear—the NST," *J. Korean Astron. Soc.* **36**, 125–133 (2003).
7. J. P. McMullin et al., "Construction status of the Daniel K. Inouye Solar Telescope," *Proc. SPIE* **9906**, 99061B (2016).
8. S. A. Mattews et al., "The European solar telescope (EST)," *Proc. SPIE* **9908**, 990809 (2016).
9. S. S. Hasana et al., "NLST: India's National Large Solar Telescope," *Astron. Nachr.* **331**(6), 628–635 (2010).
10. C. Rao et al., "1.8-m solar telescope in China: Chinese Large Solar Telescope," *J. Astron. Telesc. Instrum. Syst.* **1**(2), 024001 (2015).
11. L. Zago, "An engineering handbook for local and dome seeing," *Proc. SPIE* **2871**, 726–736 (1997).
12. M. Iye et al., "Evaluation of seeing on a 62-cm mirror," *Publ. Astron. Soc. Pac.* **103**(665), 712–722 (1991).
13. P. R. Wood and S. G. Ryan, "Effects on seeing at the Anglo-Australian Telescope of temperature differences between outside air, dome air and mirror," *Publ. Astron. Soc. Aust.* **12**(1), 95–96 (1995).
14. J. R. P. Angel, A. Y. S. Cheng, and N. J. Woolf, "Steps toward 8m honeycomb mirrors VI. Thermal control," *Proc. SPIE* **571**, 123–130 (1985).
15. R. Greenhalgh, L. M. Stepp, and E. R. Hansen, "The Gemini primary mirror thermal management system," *Proc. SPIE* **2199**, 911–921 (1994).
16. B. Bohannan, E. T. Pearson, and D. Hagelbarger, "Thermal control of classical astronomical primary mirrors," *Proc. SPIE* **4004**, 406–416 (2000).
17. P. Emde et al., "Thermal design features of the solar telescope GREGOR," *Proc. SPIE* **5495**, 238–246 (2004).
18. E. Hansen, S. Bulau, and L. Phelps, "Advanced technology solar telescope M1 thermal control system design, modeling and prototype testing," *Proc. SPIE* **7012**, 701233 (2008).
19. Y. Liu et al., "Active thermal control for the 1.8-m primary mirror of the solar telescope CLST," *Proc. SPIE* **9906**, 99061C (2016).
20. C. Rao et al., "Progress on the 1.8 m solar telescope: the CLST," *Proc. SPIE* **9906**, 990647 (2016).
21. C. Rao et al., "1.8-M solar telescope in China: the CLST," *Proc. SPIE* **9145**, 914529 (2014).
22. H. Matin, "Heat and mass transfer between impinging gas jets and solid surfaces," *Adv. Heat Transfer* **13**, 1–60 (1977).
23. S. Yang and W. Tao, *Heat Transfer*, version 4, chapter 1, pp. 595, Higher Education Press, Beijing, China (2006).
24. R. K. Banyal, B. Ravindra, and S. Chatterjee, "Opto-thermal analysis of a light-weighted mirror for solar telescope," *Opt. Express* **21**(16), 7065–7081 (2013).
25. F. M. Göttsche and F. S. Olesen, "Modeling of diurnal cycles of brightness temperature extracted from METEOSAT data," *Remote Sens. Environ.* **76**, 337–348 (2001).

Naiting Gu is an associate professor at the Institute of Optics Electronics (IOE), Chinese Academy of Science (CAS). He received his BS degree in optics from Chongqing University in 2007, and his PhD degree in optical engineering from the University of CAS in 2012. He is the author of more than 30 journal papers and has written one book chapter. His current research interests include solar telescope systems, interferometry, polarization imaging, thermal control, and adaptive optics systems.

Cheng Li is an associate professor at IOE, CAS. She received her BS and MS degrees in mechanical engineering from Sichuan University in 2006 and 2012, respectively. Her current research interest is in mechanical design for ground-based telescopes.

Yuntao Cheng is an associate professor at IOE, CAS. He received his MS degree in mechatronics engineering from Harbin Institute of Technology in 2006. He has researched mirror blank design and engineering for over 10 years. His current research interest is in mirror blank design for large ground-based telescopes.

Changhui Rao is a professor at IOE, CAS. He received his BS degree in optical metrology from Wuhan University in 1993 and his PhD degree in optical engineering from the University of CAS in 2001. He has researched on adaptive optics technology for over 20 years. He is the author of more than 200 journal papers and has written two book chapters. His current research interests include solar telescope systems, adaptive optics, and solar observation with high-resolution.